ESC European Society of Cardiology

Cardiovascular Research (2017) **113**, 1161–1172
doi:10.1093/cvr/cvx087

Increased passive stiffness promotes diastolic dysfunction despite improved Ca^{2+} handling during left ventricular concentric hypertrophy

Åsmund T. Røe[1]*, Jan Magnus Aronsen[1,2], Kristine Skårdal[1], Nazha Hamdani[3], Wolfgang A. Linke[3], Håvard E. Danielsen[4,5,6], Ole M. Sejersted[1], Ivar Sjaastad[1], and William E. Louch[1]

[1]Institute for Experimental Medical Research, Oslo University Hospital and University of Oslo, Ullevål, Kirkeveien 166, NO-0407 Oslo, Norway; [2]Bjørknes College, Oslo, Norway; [3]Department of Cardiovascular Physiology, Ruhr University Bochum, Bochum, Germany; [4]Institute for Cancer Genetics and Informatics, Oslo University Hospital, Oslo, Norway; [5]Centre for Cancer Biomedicine, University of Oslo, Oslo, Norway; and [6]Nuffield Division of Clinical Laboratory Sciences, University of Oxford, Oxford, UK

Received 13 December 2016; revised 20 February 2017; editorial decision 2 May 2017; accepted 3 May 2017; online publish-ahead-of-print 4 May 2017

Time for primary review: 54 days

Aims Concentric hypertrophy following pressure-overload is linked to preserved systolic function but impaired diastolic function, and is an important substrate for heart failure with preserved ejection fraction. While increased passive stiffness of the myocardium is a suggested mechanism underlying diastolic dysfunction in these hearts, the contribution of *active* diastolic Ca^{2+} cycling in cardiomyocytes remains unclear. In this study, we sought to dissect contributions of passive and active mechanisms to diastolic dysfunction in the concentrically hypertrophied heart following pressure-overload.

Methods and results Rats were subjected to aortic banding (AB), and experiments were performed 6 weeks after surgery using sham-operated rats as controls. *In vivo* ejection fraction and fractional shortening were normal, confirming preservation of systolic function. Left ventricular concentric hypertrophy and diastolic dysfunction following AB were indicated by thickening of the ventricular wall, reduced peak early diastolic tissue velocity, and higher E/e' values. Slowed relaxation was also observed in left ventricular muscle strips isolated from AB hearts, during both isometric and isotonic stimulation, and accompanied by increases in passive tension, viscosity, and extracellular collagen. An altered titin phosphorylation profile was observed with hypophosphorylation of the phosphosites S4080 and S3991 sites within the N2Bus, and S12884 within the PEVK region. Increased titin-based stiffness was confirmed by salt-extraction experiments. In contrast, isolated, unloaded cardiomyocytes exhibited accelerated relaxation in AB compared to sham, and less contracture at high pacing frequencies. Parallel enhancement of diastolic Ca^{2+} handling was observed, with augmented NCX and SERCA2 activity and lowered resting cytosolic [Ca^{2+}].

Conclusion In the hypertrophied heart with preserved systolic function, *in vivo* diastolic dysfunction develops as cardiac fibrosis and alterations in titin phosphorylation compromise left ventricular compliance, and despite compensatory changes in cardiomyocyte Ca^{2+} homeostasis.

Keywords Diastolic dysfunction • Concentric hypertrophy • Ca^{2+} homeostasis • Titin • Collagen

1. Introduction

Heart failure is a crippling disease caused by reduced ability of the heart to pump sufficient blood to meet the metabolic demands of the body. Cardiac output is dependent on both ventricular contractile force during systole, and ventricular filling during diastole. In approximately 50% of heart failure patients, systolic function is near normal, while impaired diastolic function restricts filling of the left ventricle with blood.[1] This

* Corresponding author. Tel: +47 23 01 68 00; fax: +47 23 01 67 99, E-mail: a.t.roe@medisin.uio.no

condition is termed heart failure with preserved ejection fraction (HFpEF), and represents a distinct entity from heart failure with reduced ejection fraction (HFrEF) where ventricular dilation and contractile dysfunction are central features. HFpEF is characterized by a variety of co-morbidities and haemodynamic alterations, but concentric hypertrophy of the left ventricle appears to be a common feature.[2] Concentric hypertrophy may be driven by neurohumoral activation, increased mechanical load, or cytokines associated with other co-morbidities.[2] The increase in left ventricular mass/volume ratio allows systolic function to be maintained, but yields a substrate for diastolic dysfunction which eventually may lead to HFpEF.[3] Determining the mechanistic link between concentric hypertrophy and diastolic dysfunction is therefore critical for the understanding of HFpEF pathophysiology.

Conceptually, there are two properties of the left ventricle that regulate diastolic filling. The first is *passive* stiffness which is dependent on properties of cellular and extracellular structural proteins.[1] From previous studies it is known that myocardial passive stiffness is increased in the hypertrophied heart due to deposition of extracellular collagen (fibrosis).[4] However, accumulating evidence indicates that elevated passive stiffness can also be traced to alterations in the giant cytoskeletal protein titin. Phosphorylation of titin by protein kinase A (PKA), protein kinase G (PKG), Ca^{2+}/calmodulin-dependent kinase II (CaMKII), and extracellular signal-regulated kinase 2 (ERK2) reduce its stiffness, while stiffness is increased by protein kinase C (PKC) phosphorylation.[5] Elevated passive stiffness of cardiomyocytes is reported to be especially evident in patients with HFpEF, and also in patients with aortic stenosis and diabetes mellitus.[6] However, the precise array of changes in titin post-translational modifications in these conditions is unclear, as is their overall contribution to diastolic dysfunction.

The second property which regulates diastolic ventricular filling is *active* relaxation, determined by the energy-dependent removal of Ca^{2+} from the cytosol. Ca^{2+} removal enables detachment of myosin cross-bridges during diastole, and is orchestrated by the sarcoplasmic reticulum (SR) Ca^{2+}-ATPase 2 (SERCA2), which recycles Ca^{2+} into the SR, and the Na^{+}/Ca^{2+}-exchanger (NCX) which extrudes Ca^{2+} from the cell.[7] Disrupted cardiomyocyte Ca^{2+} homeostasis involving pathologic alterations in SERCA2 and NCX activity is a key mechanism of systolic dysfunction in HFrEF, currently being targeted in emerging heart failure therapies.[8] Reduced SERCA2 and/or NCX activity also have the potential to slow relaxation and cause diastolic dysfunction, but it remains to be established whether such alterations in cardiomyocyte Ca^{2+} handling contribute to diastolic dysfunction in concentric hypertrophy where systolic function is preserved. An early study conducted by Selby and colleagues revealed that in patients with hypertrophy associated with hypertension and coronary artery disease, diastolic dysfunction was associated with higher Ca^{2+} load at high heart rates and a substantial active resting tone.[9] Moreover, recent data from a rat HFpEF model, where hypertrophy was induced by chronic kidney disease, demonstrated that *in vivo* relaxation abnormalities were associated with slower Ca^{2+} removal and impaired NCX function.[10] While these findings suggest that abnormal diastolic Ca^{2+} handling may be important for diastolic dysfunction in concentric hypertrophy, it is unclear whether such changes are specific to the underlying aetiologies in these studies, or indicative of concentric hypertrophy itself. The main objective of our study was therefore to determine whether alterations in diastolic Ca^{2+} handling contribute to diastolic dysfunction in concentric hypertrophy following pressure-overload, while comparing and dissecting changes in passive myocardial stiffness. Our results show that diastolic Ca^{2+} homeostasis is in fact compensated in these hearts, which acts to partially counteract passive myocardial stiffness resulting from collagen deposition and altered titin phosphorylation status.

2. Methods

An expanded methods section is available in the online supplement

2.1 Animal model

All experiments were approved by the Norwegian Animal Research Authority (FDU application 3820 and 7737) and performed in accordance with the Norwegian Animal Welfare Act and NIH Guidelines (NIH publication No. 85-23, revised 2011). Aortic banding (AB) was performed in isoflurane-anaesthetized male Wistar rats (mask ventilated with a mixture of 2.5% isoflurane, 97.5% oxygen), and sham-operated rats served as controls. Six weeks following surgery, echocardiography was performed to characterize *in vivo* cardiac function. Criterion for inclusion in the AB group was posterior wall thickening (>1.9 mm), while rats with signs of eccentric remodelling (left atrial diameter > 5.0 mm and left ventricular dilation) were excluded. To further characterize cardiac function *in vivo*, a cohort of rats underwent examination with magnetic resonance imaging (MRI).[11,12]

After *in vivo* cardiac assessment, hearts were rapidly excised from sedated animals, immediately immersed in ice-cold saline, weighed, and used for further experiments.

2.2 Muscle strip experiments

In Langendorff-perfused hearts, muscle strips (~1–1.5 mm diameter) were excised from the endocardium of the free wall and septum of left ventricle by careful dissection along the fibre direction.

Isometric force development: Left ventricular strips were mounted between metal clips in an organ bath and superfused with a Tyrode solution at 37°C, continuously bubbled with O_2 (95%) and CO_2 (5%). Strips were field stimulated at 0.5 Hz, and stretched until maximum force development. The magnitude of force development, time to peak force, and time to 50% relaxation were then recorded at 0.5, 1, 2, 4, and 6 Hz stimulation.

Isotonic contractions: In order to approximate *in vivo* conditions, a subset of strips was used for isotonic recordings. Afterload was reduced to 30% of maximal force development and shortening recorded at 1 Hz stimulation. At the completion of this protocol, strips were snap frozen in liquid nitrogen and later used for passive tension measurements.

Passive tension: For measurements of passive tension, snap frozen muscle strips were gently defrosted in ice-cold relaxing solution, skinned, and mounted between metal clips at room temperature.[13] Slack length (L_0) was defined as the maximum length where force was zero. Strips were stretched in six consecutive steps from L_0 until 1.3 L_0, tension was calculated by dividing force by cross-sectional area, and elastic and viscous stress were determined. Finally, the relative contributions of collagen and titin to myocardial stiffness were calculated by eliminating the titin contribution to elastic tension by KCl/KI extraction.

Ca^{2+} sensitivity measurements: Fresh muscle strips were skinned in relaxing solution, mounted between metal clips, and attached to a force transducer. Ca^{2+} sensitivity of the contractile apparatus (pCa_{50}) was determined by progressively increasing the Ca^{2+} concentration while recording force at 1.2 L_0.

2.3 Single cell experiments

For single cell experiments, left ventricular cardiomyocytes were isolated using the collagenase perfusion method described previously.[14] For measurements of single cell contractions and whole-cell Ca^{2+} transients, the cardiomyocytes were plated on laminin-coated coverslips on the stage of an inverted microscope and superfused with Hepes Tyrode's solution at 37°C.

Single cell contractions: Contractions were elicited by field stimulation, and cell length was recorded by video edge detection during stimulation at 0.5, 1, 2, 4, and 6 Hz.

Ca^{2+} transient measurements: Using the same stimulation protocol, Ca^{2+} transients were recorded in cardiomyocytes preincubated with 10 μM fluo 4-AM (Invitrogen, Oslo, Norway).[14] SR Ca^{2+} content was assessed by rapidly applying 10 mM caffeine, and constants for sarcolemmal Ca^{2+} extrusion and SR Ca^{2+} reuptake calculated.[15]

Resting diastolic $[Ca^{2+}]_i$, was determined in cells incubated with 10 μM Indo-1 AM (Invitrogen, Oslo, Norway), and these values were employed to calibrate fluo-4 Ca^{2+} transients as described.[16]

Patch clamp: For analysis of L-type Ca^{2+} currents, we employed the whole-cell voltage clamp technique, with discontinuous voltage clamp (8–10 kHz switching) and 1–2 MΩ glass pipettes.[15] I_{CaL} was elicited by 210-ms depolarising voltage steps from –40 to +50 mV in 10-mV increments. Action potentials were recorded in patch-clamped cells, and a 3 ms supra-threshold current injection was used to elicit action potentials at 1 Hz.

Sarcomere lengths: Sarcomere lengths were measured in resting cardiomyocytes stained with di-8-ANEPPS (10 μM, Molecular Probes, Eugene, OR) using an LSM 510 confocal scanning microscope (Zeiss).

2.4 Protein assays

Western blotting: Primary antibodies for immunoblotting were: SERCA2 (1:2500) (MA3-919, Thermo Scientific), NCX (1:500),[17] phospholamban (1:5000) (MA3-922, Thermo Scientific), phospholamban Ser16 (1:5000) (A010-12,Badrilla, Leeds, UK), phospholamban Thr17 (1:5000) (A010-13, Badrilla), CaV1.2 (1:500) (ACC-003, Almone Labs, Jerusalem, Israel) and GAPDH (1:500) (sc-20357, Santa Cruz Biotechnology Inc., Texas, USA). Secondary antibodies were anti-rabbit or anti-mouse IgG HRP linked whole antibody (GE Healthcare, Oslo, Norway). The data were normalized to sham (=100%).

Titin phosphorylation assays: 1.8% SDS-PAGE followed by Western blot was performed to measure expression and site-specific phosphorylation of titin.[18,19] Phosphoserine/phosphothreonine-specific titin antibodies were used for total titin phosphorylation. The following affinity-purified phosphosite-specific anti-titin antibodies were used: Anti-phospho-N2Bus-titin (S3991, S4043, and S4080 in mouse titin), and anti-phospho-PEVK-domain (S12742 and S12884).[18] All phospho-signals were normalized to PVDF stains and the data were normalized to sham (=100%).

PCR assays: We quantified the gene expression levels of collagen and myosin heavy chain isoforms by digital droplet PCR (ddPCR), allowing the absolute mRNA quantity of collagen type I and type III, and myosin heavy chain 6 and 7, to be determined. Data were normalized to ribosomal protein L32.

Collagen histology: Fresh cardiac tissue was immediately fixed in 4% formalin. Collagen volume fraction in Masson trichrome stained cross-sections of the left ventricle was quantified by computerized image analyses as previously described in detail.[20]

2.5 Statistics

All results are expressed as mean values ± standard error of the mean. Statistical significance was calculated by Student's *t*-test in unpaired animal data, while a nested ANOVA test was employed for muscle strip and single cell data. Two-way repeated-measurement (RM) ANOVA analysis with a post-hoc Bonferroni *t*-test was additionally used where appropriate, as indicated in the figure legends. Statistical significance was defined as $P < 0.05$.

3. Results

3.1 *In vivo* diastolic dysfunction following aortic banding

In vivo cardiac geometry and function for aortic banding (AB) and sham hearts were assessed by MRI and echocardiography (*Figure 1* and *Table 1*). AB resulted in concentric hypertrophy, indicated by increased left ventricular mass and wall thickness, and reduced left ventricular end-diastolic volume. Impaired diastolic function was demonstrated by reduced peak early diastolic tissue velocities (e'), as measured by echocardiography, and by higher E/e' values measured by MRI. Fractional shortening and ejection fraction were unaltered, indicating preserved systolic function in the AB group. A modest increase in left atrial diameter was observed in AB, as well as a modestly higher lung weight. Since systolic function was preserved, these latter changes may be attributed to elevated filling pressures secondary to diastolic dysfunction.

3.2 Modest slowing of relaxation in AB myocardial strips

Basic mechanical properties of left ventricular muscle strips isolated from sham and AB hearts are presented in *Figure 2*. Consistent with the observation of preserved systolic function *in vivo*, the magnitude of isometric force generation was also unchanged in AB (*Figure 2A* and *B*). A negative force-frequency response was observed in both sham and AB, in agreement with previous studies conducted at 37°C.[21] In comparison with sham, the kinetics of contraction and relaxation were slower in AB muscle strips, with observed reductions in time to peak force generation (*Figure 2C*) and time to 50% relaxation (*Figure 2D*). Similar deficits of contraction and relaxation kinetics were observed in AB muscle strips stimulated isotonically (*Figure 2E–G*). As commonly reported in left ventricular hypertrophy, an α to β isoform shift in myosin heavy chain expression was observed (see Supplementary material online, *Figure S3D*). These data support the premise that diastolic dysfunction after AB is linked to intrinsic alterations in myocardial mechanics.

3.3 Increased myocardial passive tension in AB - role of collagen and titin

Passive stress of the myocardium was assessed by recording tension during progressive stretch. Passive myocardial tension was higher in myocardial strips from AB rats, evidenced by both steeper passive length-tension relationships, and increased tissue viscosity (*Figure 3A–C*). Passive tension of the myocardium is dependent on both cardiomyocyte titin properties and extracellular collagen. While total titin phosphorylation was unaltered in AB compared to sham (*Figure 4A*), we observed alterations at specific, conserved phosphosites in the N2Bus and PEVK domains. The PKA/ERK2-dependent S3991 and PKG-dependent S4080 sites on the N2Bus were hypophosphorylated in AB, whereas the CaMKII phosphosite S4043 was unaltered. Within the PEVK region, the

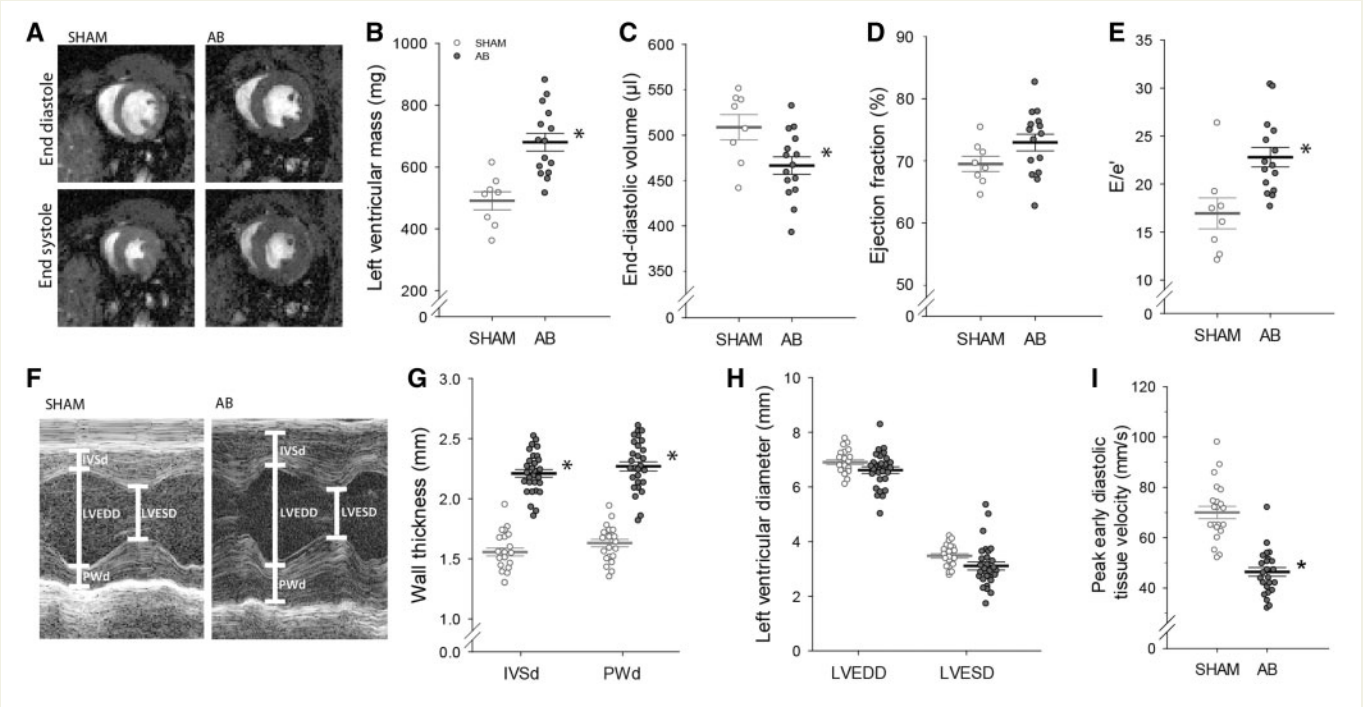

Figure 1 Concentric hypertrophy and diastolic dysfunction observed *in vivo* following AB. (*A*) Representative cine MRI pictures. (*B–E*) Cine and phase-contrast MRI revealed higher left ventricular mass (*B*), lower end-diastolic volume (*C*), preserved ejection fraction (*D*), and higher E/e' (*E*) in AB. ($n = 8,15$ in sham, AB). Cardiac structure and function were additionally examined by echocardiography (*F–I*). Representative M-mode recordings (*F*) and mean measurements revealed thickening of the ventricular wall (*G*) and maintained end-diastolic diameter (*H*), confirming the presence of concentric hypertrophy in AB. Tissue Doppler measurements showed reduced diastolic tissue velocity in AB compare to sham (*I*) ($n = 23,29$ in sham, AB). (*= $P < 0.05$ vs. sham calculated with student *t*-test). (*PWd= diastolic posterior wall diameter, AWd= diastolic anterior wall diameter, LVED = left ventricular end-diastolic diameter, LVESD = left ventricular end-systolic diameter*).

Table 1 Animal characteristics

	SHAM	AB
POST-MORTEM ANALYSES ($n_{animals}$ = 26, 38)		
- Body weight (g):	412.4 ± 11.7	406.3 ± 10.2
- Left ventricular weight (g):	1.31 ± 0.05	1.88 ± 0.08*
- Lung weight (g):	1.46 ± 0.04	2.04 ± 0.14*
- Left ventricular/body weight (mg/g):	3.19 ± 0.11	4.64 ± 0.19*
- Lung/body weight (mg/g):	3.62 ± 0.12	5.17 ± 0.41*
ECHOCARDIOGRAPHIC ANALYSES ($n_{animals}$ = 23, 29)		
- Heart rate (min^{-1})	399.0 ± 7.7	390.3 ± 7.3
- Left atrial diameter (mm):	3.49 ± 0.07	4.05 ± 0.12*
- Fractional shortening (%):	49.6 ± 1.2	53.4 ± 1.6
- Peak mitral flow (mm/s)	921.2 ± 26.0	1014.9 ± 36.6*
MRI ANALYSES ($n_{animals}$ = 8, 15)		
- Heart rate (min^{-1})	399.7 ± 6.5	395.3 ± 7.9
- Peak mitral flow (mm/s)	1039 ± 27	1164 ± 64
- e' (mm/s)	64.7 ± 5.5	51.9 ± 3.1*

(*=$P < 0.05$ vs. sham measured by student *t*-test).

PKC/CaMKII S12884 phosphosite was hypophosphorylated, although a tendency towards increased phosphorylation at the PKC S12742 phosphosite was observed ($P = 0.1$). Overall, these modifications are consistent with higher titin stiffness in AB than in sham, particularly within the N2Bus.[5] Indeed, KCl/KI extraction experiments identified a markedly increased contribution of cytoskeletal stiffness to overall passive tension in AB hearts (*Figure 3D*).

Levels of collagen type I and type III mRNA were increased following AB, suggesting marked extracellular fibrosis (*Figure 4C*). This finding was supported by histologic examination of left ventricular sections, which revealed collagen deposition to be significantly higher in the extracellular matrix of AB hearts (*Figure 4B* and *D*).

3.4 Enhanced relaxation in single cells after AB

To investigate mechanical properties at the cellular level, in the absence of the influence of the extracellular matrix, we measured single cell contractions for a range of stimulation frequencies. As these cells were unloaded, higher titin stiffness is not anticipated to impair relaxation; rather a stiffened titin protein can augment recoil at short sarcomere lengths.[22] The magnitude of contraction was unaltered in AB at all pacing frequencies, consistent with normal systolic function (*Figure 5A* and *B*). Contraction and relaxation in single cardiomyocytes were significantly accelerated in AB compared to sham (*Figure 5C* and *D*). AB cardiomyocytes also exhibited less diastolic contracture with increasing pacing frequencies, and resting diastolic sarcomere lengths tended to be longer (sham 1.786 ± 0.027 µm vs. AB 1.836 ± 0.013 µm, $P = 0.06$). Such changes in cardiomyocyte relaxation would be expected to be compensatory during all phases of diastole, as accelerated rate and increased extent of relaxation aids filling throughout early and late diastole.[7]

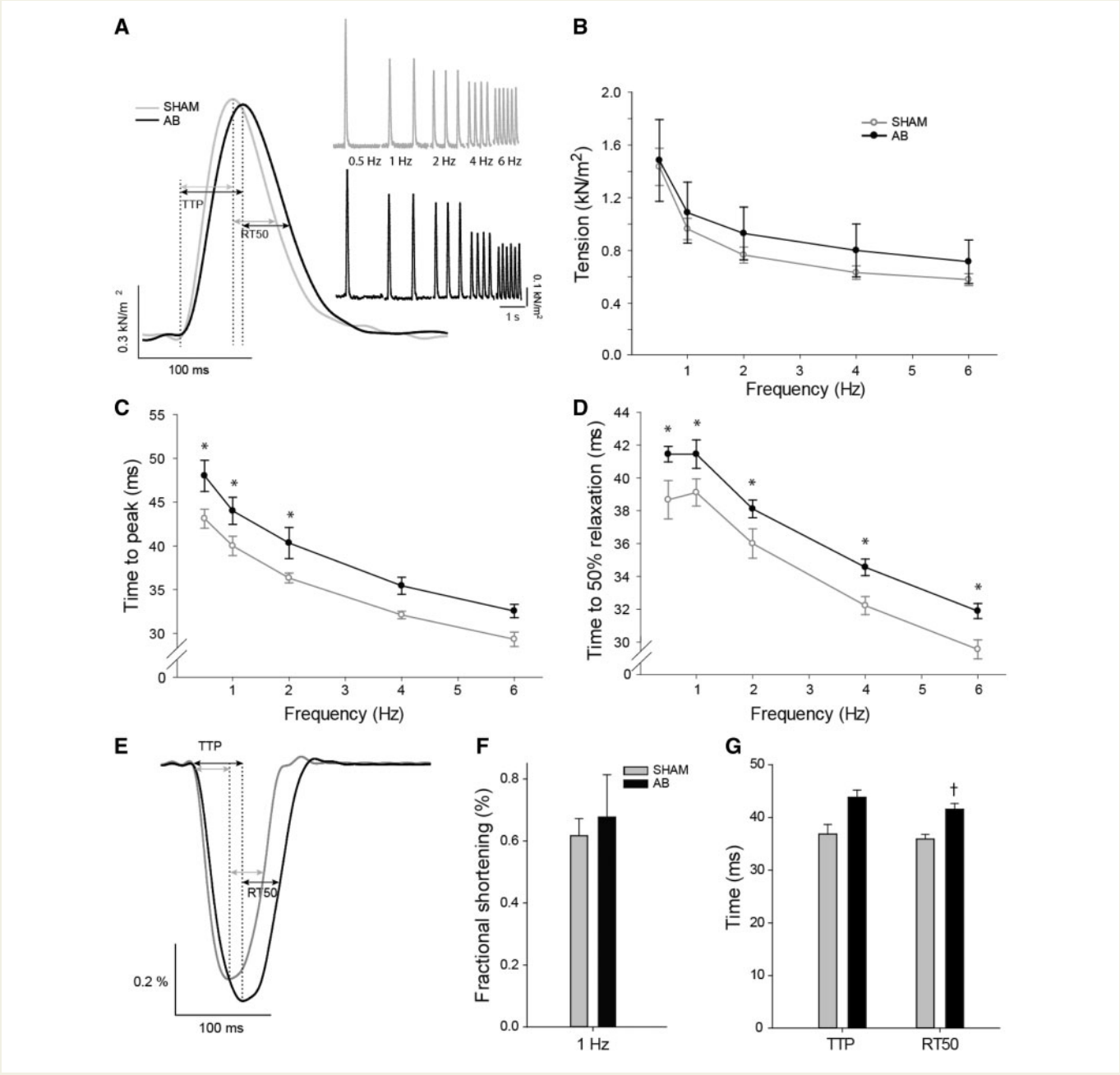

Figure 2 Slowing of relaxation in muscle strips from AB hearts. Representative isometric (*A*) and isotonic (*E*) contractions from a sham and AB muscle strip at 1 Hz. The magnitude of isometric force development (*B*) and isotonic shortening (*F*) were preserved in AB. Time to peak isometric force (*C*) and isotonic shortening (*G*), and time to 50% relaxation (*D* and *G*) were prolonged in AB. ($n_{isometric}$= 9,9 strips from 3,3 hearts in sham, AB, $n_{isotonic}$= 11,8 strips from 3,3 hearts in sham, AB). (*= $P < 0.05$ vs. sham calculated with two-way RM-ANOVA with a post-hoc Bonferroni *t*-test (B-D), †=$P < 0.05$ vs. sham calculated with nested ANOVA (B-D, F, G)). *(TTP = time to peak; RT50 = time to 50% relaxation).*

4. Enhanced diastolic Ca^{2+} cycling after AB

To determine the mechanisms underlying enhanced relaxation in isolated AB cardiomyocytes, Ca^{2+} handling was examined by whole-cell Ca^{2+} fluorescence, and patch clamp. Ca^{2+} transient magnitude was reduced in AB at higher stimulation frequencies (*Figure 6A* and *B*). In agreement with improved cellular relaxation, diastolic Ca^{2+} handling was markedly enhanced in AB cardiomyocytes, as evidenced by faster decline of the Ca^{2+} transient across a range of pacing frequencies (0.5-6 Hz, *Figure 6A* and *D*). Furthermore, resting $[Ca^{2+}]_i$ was lower and there was less accumulation of diastolic Ca^{2+} at high pacing frequencies in AB (*Figure 6E*). Function of the two main systems for cytosolic Ca^{2+} removal, NCX and SERCA2, was assessed by rapid caffeine application (*Figure 7A*). Rate constants of both SR Ca^{2+} recycling and sarcolemmal Ca^{2+} extrusion were higher in AB (*Figure 7C* and *D*), indicating enhanced SERCA2 and NCX activity, respectively. Increased Ca^{2+} cycling by these proteins did not result from alterations in protein levels, as

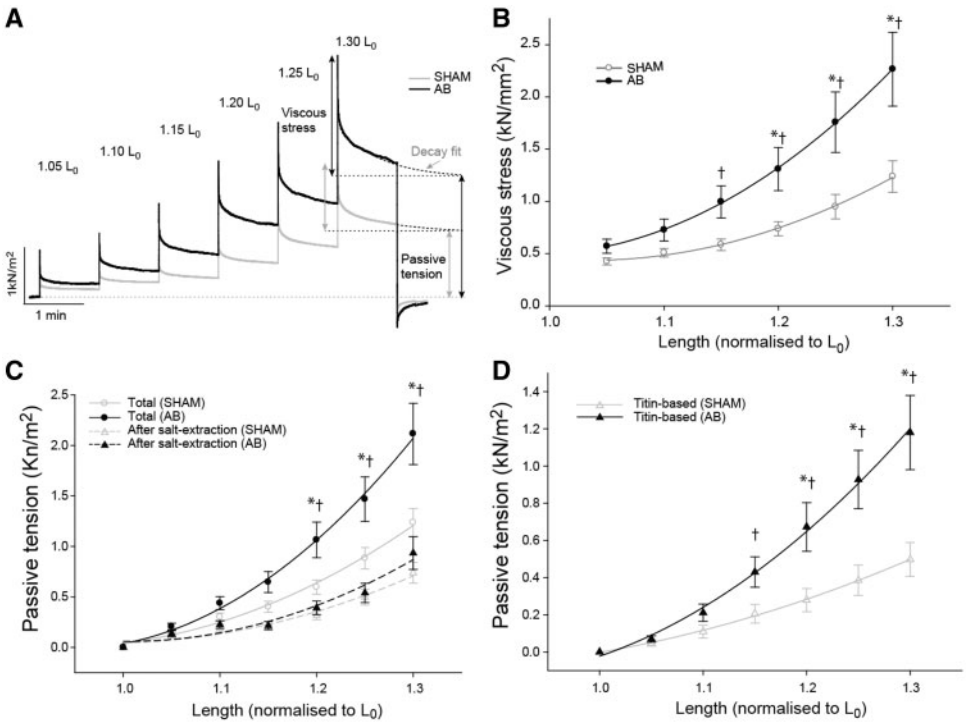

Figure 3 Higher myocardial passive stiffness. (*A*) Muscle strips were stretched in a step-wise manner. Viscous stress was greater in AB than sham, as indicated by a larger overshoot of tension above baseline during rapid stretch (*B*), and the length-tension relationship was increased in the AB myocardium (solid lines) (*C*). Salt extraction of the myofilaments resulted in a proportionally greater reduction in passive tension in AB than Sham (dotted lines), with difference curves used to estimate the titin contribution (*D*). Curves are second-order polynomial fits to the mean values. (n = 11,11 strips from 3,3 hearts in sham, AB) (*=$P < 0.05$ vs. sham calculated with two-way RM-ANOVA with a post-hoc Bonferroni t-test, †=$P < 0.05$ vs. sham calculated with nested ANOVA).

indicated by Western blots of SERCA2a, phospholamban, and NCX (see Supplementary material online, *Figure S2*).

NCX competes with SERCA2 for the same pool of cytosolic Ca^{2+}, and consistent with enhanced NCX function the SR Ca^{2+} content was reduced in AB (*Figure 7B*). While diminished SR content is expected to dramatically reduce Ca^{2+} transient magnitude, such effects were partly offset by augmentation of L-type Ca^{2+} current (*Figure 7E* and *F*), and prolongation of the action potential (*Figure 7G* and *H*), which are expected to enhance SR Ca^{2+} release.

5. Discussion

In this study, we present insights into the contribution of active relaxation and passive stiffness to diastolic dysfunction in the concentrically hypertrophied heart with preserved systolic function. Aortic banding (AB) in rats induced concentric hypertrophy and diastolic dysfunction *in vivo*, which was associated with slowing of relaxation in left ventricular muscle strips *ex vivo* compared to sham-operated controls. In contrast, relaxation in individual cardiomyocytes was enhanced. Accelerated Ca^{2+} removal during diastole, mediated by enhanced NCX and SERCA2 activity, appeared to be key to this compensatory response. Thus, diastolic dysfunction following concentric hypertrophy was not a result of altered diastolic Ca^{2+} homeostasis, but rather due to higher myocardial passive stiffness.

The results of this study contribute to ongoing efforts to unravel the causal link between concentric hypertrophy and diastolic dysfunction. Concentric hypertrophy, as defined by a decrease in the ventricular volume/mass ratio, is commonly observed following elevated left ventricular afterload. This remodelling process allows systolic function to be maintained, but yields a substrate for diastolic dysfunction.[3] In line with this, our rat model of pressure-overload is associated with the development of concentric hypertrophy accompanied by slowing of early diastolic lengthening (e') and elevated filling pressures, but preserved systolic function *in vivo*. Thus, we feel confident that we have employed a robust model of diastolic dysfunction. Interest in models of diastolic dysfunction has increased in recent years due to growing awareness of the prevalence of HFpEF. However, acceptable animal models of HFpEF have proved difficult to establish as they often poorly reflect the diversity in aetiologies and various co-morbidities associated with human HFpEF. Indeed, our AB model should be regarded as a model of diastolic dysfunction and not HFpEF. However, among the complexity of human HFpEF pathophysiology, concentric hypertrophy of the left ventricle appears to be a common and important feature, and aortic stenosis may be a trigger for HFpEF in a subset of patients.[23] Thus, identifying the driving mechanisms of diastolic dysfunction in concentric hypertrophy models will have implications for understanding HFpEF pathophysiology, and future work should be aimed at unravelling the time course of how this dysfunction unfolds.

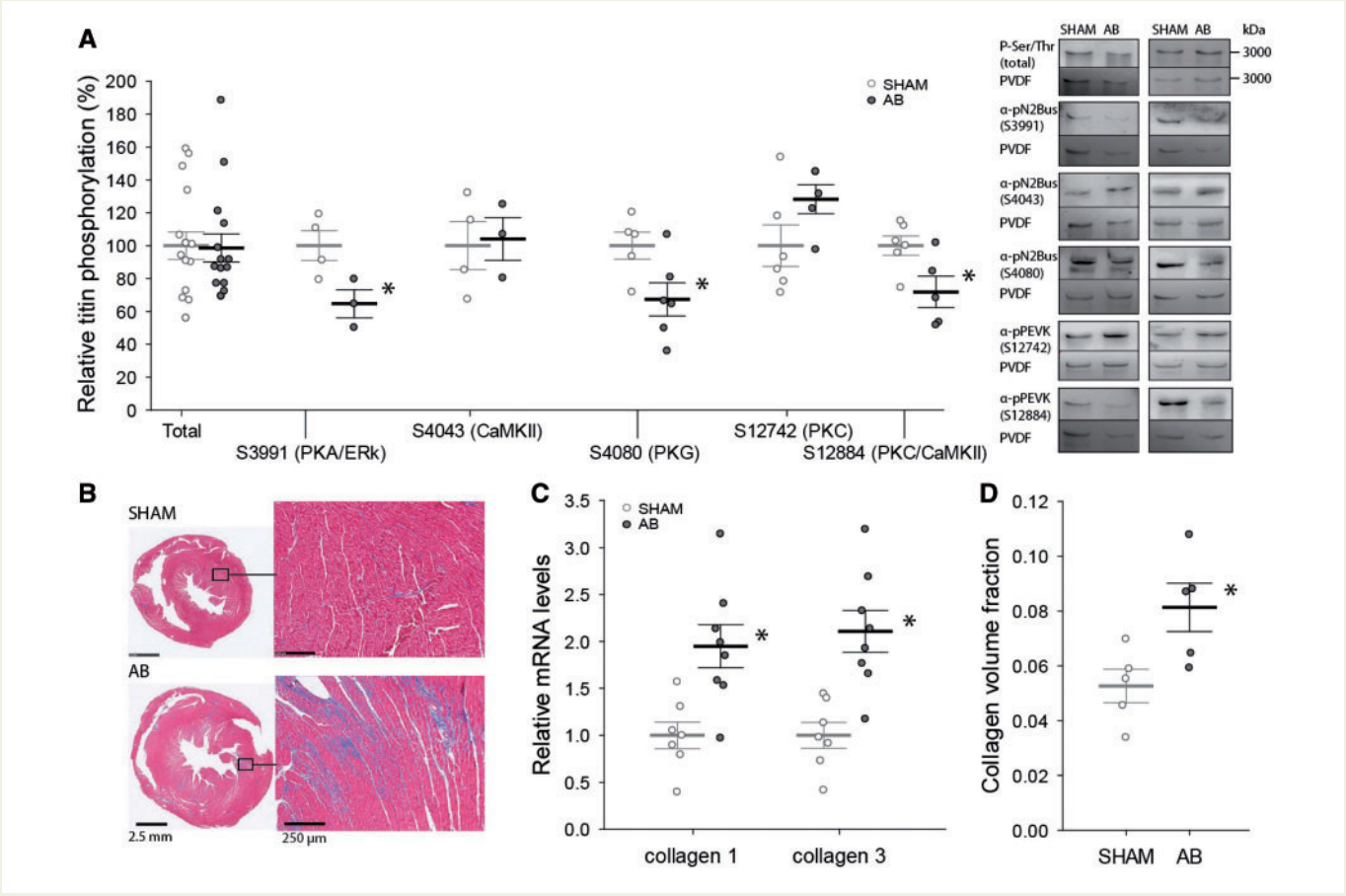

Figure 4 Left ventricular fibrosis and altered titin phosphorylation. (*A*) Scatter plots (left) from individual hearts showing total and site-specific phosphorylation of titin, corroborated by representative Western blots with PVDF stains as quality controls (right) (all stains at 3000 kDa). (*B*) Representative examples of Masson's stained left ventricular cross-sections with collagen stained blue. (*C*) Levels of collagen type I and type III mRNA were elevated (7,8 hearts in sham, AB). (*D*) Collagen volume fraction, calculated from Masson's stained left ventricular cross-sections, was increased in AB (5,5 hearts in sham, AB). (*=$P < 0.05$ vs. sham calculated with student *t*-test).

5.1 Active mechanisms of diastolic dysfunction

Cardiomyocyte contraction and active relaxation are dependent on cellular Ca^{2+} homeostasis. Disrupted Ca^{2+} handling is a main mechanism of contractile dysfunction in HFrEF, and also contributes to diastolic dysfunction in this condition.[7,8] While HFrEF is associated with eccentric remodelling of the left ventricle, Selby *et al.*[9] indicated that abnormalities in active Ca^{2+}-dependent relaxation also contributed to diastolic dysfunction in human hypertrophied hearts with preserved systolic function. Specifically, they observed elevated resting muscle tension despite normal myofilament Ca^{2+} sensitivity, which was present even in the absence of electrical stimulation. Such effects are consistent with impaired Ca^{2+} extrusion by NCX, since NCX activity alone sets resting Ca^{2+} levels in unstimulated cells.[7] Similarly, a recent study in a nephrectomized rat model of HFpEF demonstrated slowed cardiomyocyte relaxation associated with reduced NCX-mediated Ca^{2+} removal.[10] In contrast, our present results show that pressure-overload induced concentric hypertrophy in the absence of other comorbidities is associated with improved cardiomyocyte relaxation and augmented Ca^{2+} extrusion by both NCX and SERCA2. NCX is a key determinant of resting diastolic Ca^{2+} levels, [7] and enhanced NCX activity in AB cardiomyocytes is in keeping with lower diastolic $[Ca^{2+}]_i$ and longer resting sarcomere lengths. Lower diastolic $[Ca^{2+}]_i$ reduces active diastolic tone even during resting conditions,[24] and this effect is augmented at higher pacing frequencies when diastolic $[Ca^{2+}]_i$ rises. A compensatory role of enhanced NCX function has indeed been demonstrated in HFrEF patients where greater NCX activity rescued diastolic function.[25] While NCX is expected to contribute to lower resting $[Ca^{2+}]_i$ in AB, enhanced rates of Ca^{2+} transient decline, with accelerated cardiomyocyte relaxation, are likely predominantly due to augmented SERCA2 activity.[7] Therefore, enhanced NCX function in AB together with augmented SERCA2 activity can be viewed as compensatory responses which oppose restrictions on diastolic function due to passive stiffening of the myocardium. It appears then that pressure-overload induced concentric hypertrophy is not in and of itself linked to disrupted diastolic Ca^{2+} homeostasis, which contrasts with previous hypertrophy results in multi-morbid patients[9] and chronic kidney disease in rats with HFpEF.[10] This view emphasises the importance of a phenotype-specific approach to diastolic dysfunction, and supports the new HFpEF paradigm proposed by Paulus *et al.*,[26] in which extracardiac co-morbidities and systemic inflammation, rather

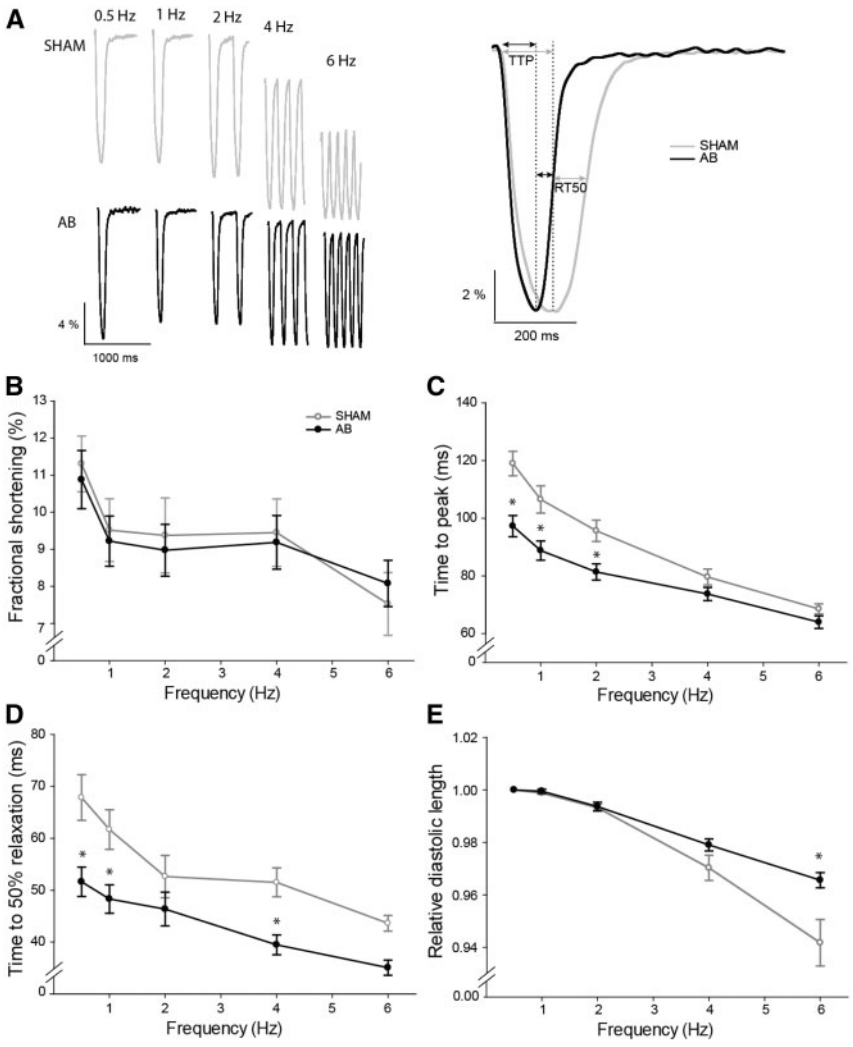

Figure 5 Enhanced relaxation in single cardiomyocytes. (*A*) Representative contractions of single cardiomyocytes for a range of stimulation frequencies (normalized to diastolic cell length at 0.5 Hz), with 1 Hz examples in greater detail. (*B*) Fractional shortening was preserved in AB. (*C*) AB cardiomyocytes contracted more rapidly in AB than sham, with reduced values for time to peak shortening. (*D*) Faster relaxation in AB cardiomyocytes, evidenced by shorter time to 50% relaxation. (*E*) AB cardiomyocytes exhibited less contracture with increasing pacing frequencies (normalized to resting cell length). (n = 18,17 cells from 3,3 hearts in sham, AB). (*=P < 0.05 vs. sham calculated with two-way RM-ANOVA with a post-hoc Bonferroni t-test, †=P < 0.05 vs. sham calculated with nested ANOVA). *(TTP = time to peak; RT50 = time to 50% relaxation).*

than direct cardiac insults, are proposed to drive the progression of HFpEF.

Augmentation of NCX activity in AB was observed despite maintained protein levels (see Supplementary material online, *Figure S2*). Augmented NCX-mediated Ca^{2+} extrusion in AB may therefore result from alterations in local cytosolic Na^{+} or Ca^{2+} levels,[27] altered NCX cleavage,[28] or reduced inhibition from phospholemman.[29] Such mechanisms have not been presently investigated. Similarly, augmented SERCA2 activity in AB was not explained by expression levels of SERCA2, phospholamban, or phospholamban phosphorylation status (see Supplementary material online, *Figure S2*). Additional SERCA2 regulatory mechanisms not presently investigated include direct regulation by PDE3A and DWORF.[30,31]

Beyond compensations in diastolic Ca^{2+} homeostasis, we additionally observed an intriguing combination of cellular-level alterations which maintained systolic function. NCX competes with SERCA2 for the same pool of cytosolic Ca^{2+}, and in conditions such as HFrEF enhanced NCX function has often been reported to occur at the expense of contractile function due to depletion of cellular Ca^{2+} stores.[27] However, higher NCX activity was largely opposed by enhanced SERCA2 function in AB cells, which limited reduction in SR content. Reduced SR Ca^{2+} release is known to attenuate the inactivation of L-type Ca^{2+} channels, and the resulting increases in baseline L-type Ca^{2+} current and action potential duration observed in AB cardiomyocytes are expected to augment triggered Ca^{2+} release.[32,33] Previously reported reductions in repolarising K^{+} currents following pressure-overload[34] may additionally contribute to action potential prolongation. Despite the longer action potential, the overall magnitude of the Ca^{2+} transient still remained somewhat smaller in AB at high stimulation frequencies. However, single cardiomyocyte contraction magnitude was preserved, suggesting that the sensitivity of

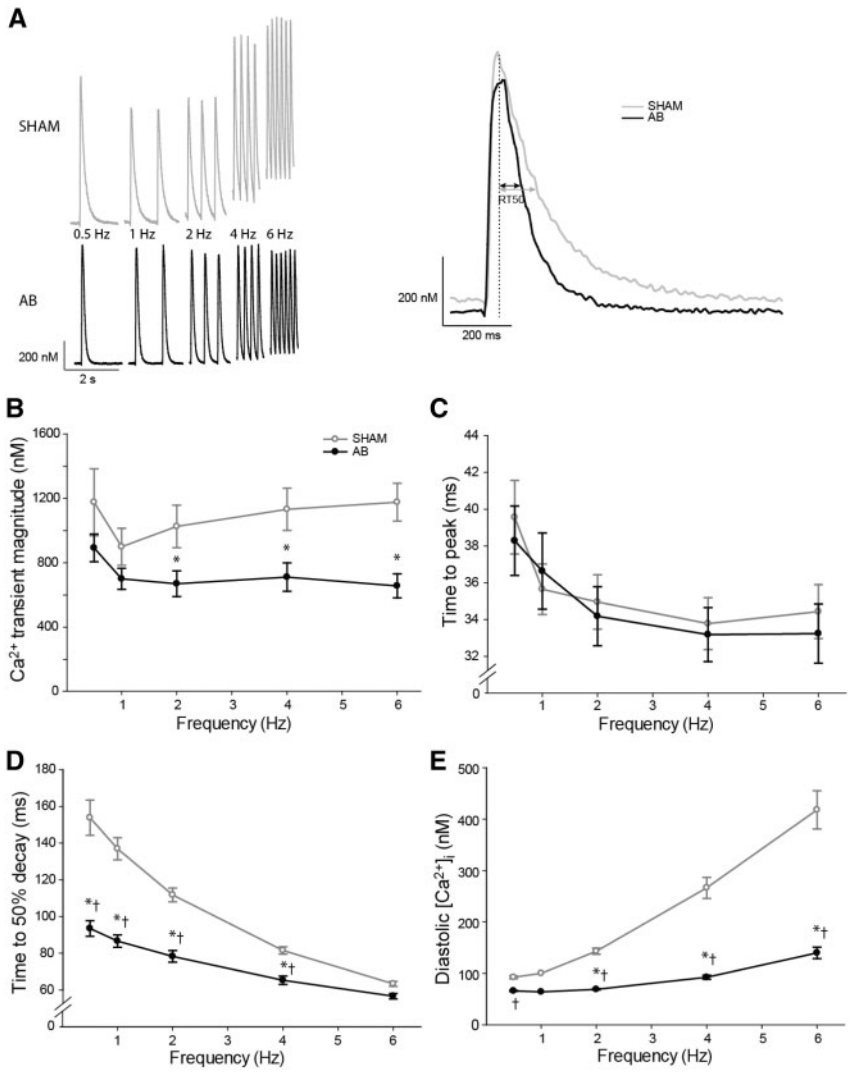

Figure 6 Compensated diastolic Ca^{2+} cycling in cardiomyocytes. (*A*) Representative Ca^{2+} transients. While Ca^{2+} transient magnitude was somewhat lower in AB than sham (*B*), time to peak of the transient was unchanged (*C*), and time to 50% decline was reduced (*D*). (*E*) Diastolic Ca^{2+} levels were lower in AB, with less accumulation of resting [Ca^{2+}] at high pacing frequencies. ($n = 23,21$ cells from 5,3 hearts in sham, AB). (*=$P < 0.05$ vs. sham calculated with two-way RM-ANOVA with a post-hoc Bonferroni *t*-test (B-E), †=$P < 0.05$ vs. sham calculated with nested ANOVA (B-E)). *(TTP = time to peak; RT50 = time to 50% relaxation)*.

the myofilaments to Ca^{2+} may be increased in AB. Although force-Ca^{2+} relationships recorded in permeabilized muscle were similar in sham and AB (see Supplementary material online, *Figure S3*), we cannot exclude that the permeabilization process and/or lack of electrical stimulation in these experiments precluded critical myofilament post-translational modifications present in intact cells. For example, CaMKII is activated at higher pacing rates, and known to increase myofilament sensitivity by phosphorylation of myosin binding protein C.[35]

What causes compensatory alterations in cardiomyocyte Ca^{2+} homeostasis during some conditions, as in the present AB model, but detrimental changes in other conditions such as HFrEF?[8,27] In an effort to identify the specific triggers, we recently investigated the role of ventricular wall stress in regulating cardiomyocyte structure and function.[36] We found that elevated wall stress and high preload trigger disruption of cardiomyocyte t-tubules and systolic Ca^{2+} release in post-infarction hearts. Concentric hypertrophy on the other hand, acts to reduce wall stress according to LaPlace's law. Thus, we believe that while volume overload and dilation of the left ventricle leads to cardiomyocyte dysfunction via increased wall stress, elevated afterload leads to wall thickening, maintained wall stress, and adaptive remodelling of Ca^{2+} homeostasis. Besides mechanosensing, neurohumoral activation is also known to trigger remodelling, and differences in renin-angiotensin-aldosterone signalling and/or sympathetic signalling may additionally contribute to different remodelling.[2]

5.2 Passive mechanisms of diastolic dysfunction

The supra-normal relaxation observed in isolated AB myocytes strongly suggests that passive mechanisms were responsible for the impaired

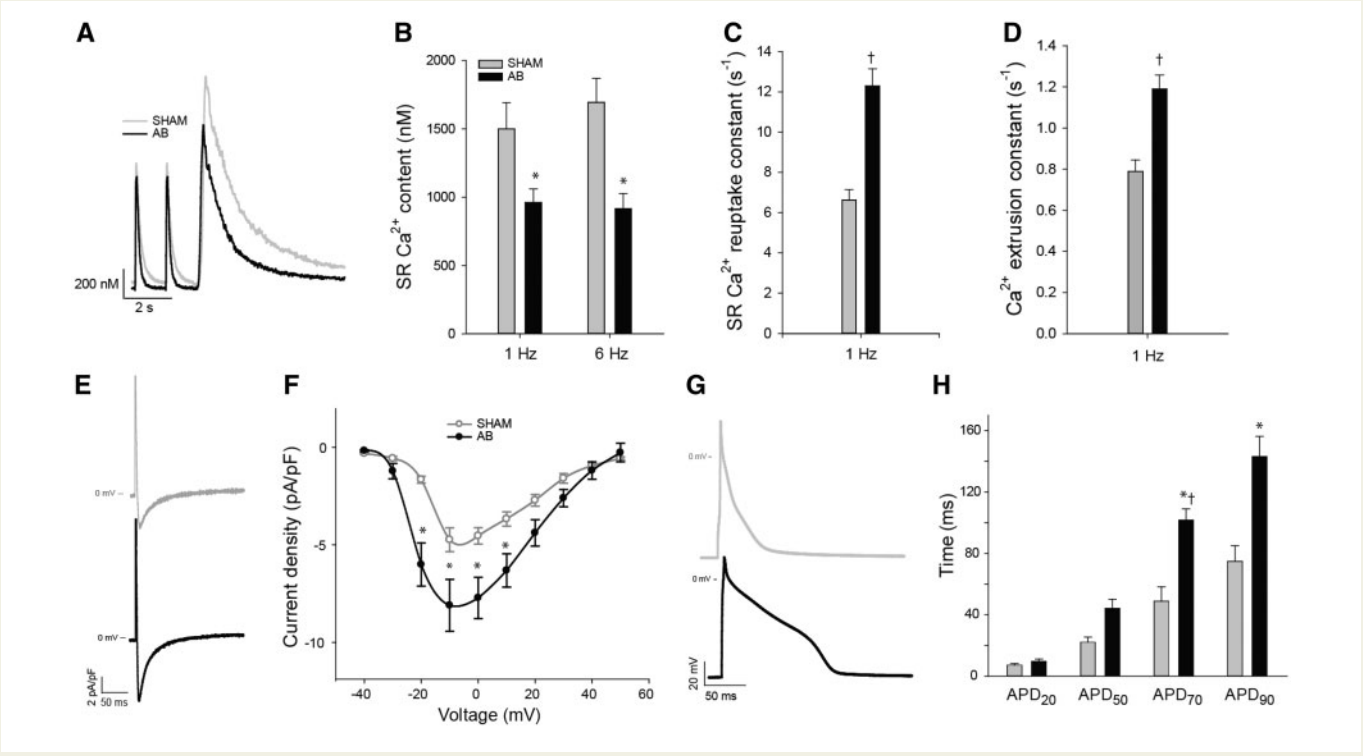

Figure 7 Enhanced fluxes of Ca^{2+} through NCX, SERCA2, and LTCC. (*A*) Representative caffeine responses. (*B*) The magnitude of the caffeine-induced Ca^{2+} release was reduced in AB vs. sham, suggesting lower SR Ca^{2+} content. (*C*) SR Ca^{2+} reuptake constant was higher in AB, indicating enhanced SERCA2 function. (*D*) The sarcolemmal Ca^{2+} extrusion constant was higher in AB, indicating enhanced NCX function. L-type Ca^{2+} current was larger in AB compared to sham, as indicated by representative current traces (*E*, step to 0 mV) and the mean current-voltage relationship (*F*). Action potentials were prolonged in AB, as demonstrated by representative recordings (*G*) and mean data at 50, 70, and 90% repolarization (*H*). (B-D: $n = 24,23$ cells from 5,3 hearts in sham, AB, E-G: $n = 6,9$ cells from 3,3 hearts in sham, AB). (*=$P < 0.05$ vs. sham calculated with two-way RM-ANOVA with a post-hoc Bonferroni *t*-test (B, F, H), †=$P < 0.05$ vs. sham calculated with nested ANOVA (B-D, F, H)). *(APD = action potential duration).*

diastolic function present in AB hearts. Indeed, consistent with previous studies, we observed higher myocardial passive tension in muscles isolated from hypertrophied hearts.[4] Myocardial stiffness describes the extent to which the tissue develops tension and resists deformation in response to stretch, and is dependent on both the length of stretch (passive elastic tension) and the rate of stretch (viscosity). Whether myocardial stiffening results from increased deposition of extracellular collagen or alterations in cellular titin stiffness has been a conflicting point in previous studies.[37,38] In the AB model, we found cardiomyocyte titin phosphorylation to be altered in a manner known to increase cardiomyocyte passive tension, with hypophosphorylation of specific PKA/ERK2 and PKG phosphosites within the N2Bus (S3991 and S4080, respectively).[5,18,19,39] This finding is consistent with previous results in models and patients with HFpEF or aortic stenosis, in which *ex vivo* PKA or PKG treatment corrected the pathologically elevated cardiomyocyte stiffness.[6,40] Phosphorylation changes within the PEVK region were less clearly pathological, as the PKC/CaMKII S12884 phosphosite was hypophosphorylated which has been suggested to reduce stiffness.[5] Such effects on PEVK stiffness could be diminished by a tendency towards increased phosphorylation at the PKC S12742 phosphosite ($P = 0.1$) in AB. We did not specifically examine titin isoform expression. However, an isoform switch is expected to have minor effects on cardiomyocyte stiffness in rat, as the stiff isoform N2B already constitutes more than 90% of titin expression in the rodent heart.[37]

In addition to altered titin phosphorylation, we observed significant fibrosis of the extracellular matrix in the hypertrophied heart. This included a marked increase in expression of collagen I and III isoforms, which are the major extracellular matrix components that determine elastic and viscous stiffness.[41] Increased deposition of extracellular collagen in our model is in line with previous studies on pressure-overload and expected to elevate passive myocardial stiffness.[6,13,41] However, our salt extraction experiments revealed that the passive tension remaining after myofilament disruption was similar in sham and AB. It should be noted that although it has previously been shown that the KCl/KI extraction protocol has minor effects on cardiac collagen,[42] we suspect that the method disrupts muscle structure, leading to underestimation of the collagen-contribution to overall stiffness. Thus, we surmise that collagen deposition is likely consequential, but that titin stiffening appeared to be the predominant contributor to increased passive tension in AB. Others have similarly previously suggested that titin is a greater contributor to myocardial stiffness than collagen within physiologic sarcomere lengths.[43]

As we examined properties of diastolic function at several levels, an interpretation of the many steps is mandated. *In vivo* diastolic dysfunction was primarily evidenced by reduced peak early diastolic tissue velocities and elevated E/e'. Peak early diastolic tissue velocities reflect active relaxation but also so-called restoring force and lengthening load,[44] whereas E/e' is a parameter of filling pressure. Active relaxation and passive

stiffness were not directly assessed *in vivo*, but were instead measured in intact tissue and isolated cardiomyocytes. At the cardiomyocyte level, enhanced $Ca^{2\pm}$ removal contributed to faster re-lengthening. However, in the absence of preload increased titin stiffness likely also speeds relaxation, due to enhanced restoring force.[22] Such enhancement of diastolic function was not observed in loaded intact muscle strip experiments where the extracellular matrix was present; rather, relaxation was slowed in AB compared to sham. Thus, we propose that elevated tissue viscoelasticity in AB critically contributes not only to reduced late diastolic compliance, but also to slowing of early relaxation. Viscosity slows lengthening as there is increased resistance to rapid deformation, and elevated passive stiffness has previously been suggested to impair early relaxation.[45] In addition, and in line with previous findings in pressure-overload,[46] we observed a shift from the myosin heavy chain α isoform to the β isoform in AB (see Supplementary material online, *Figure S3D*). The β isoform exhibits several times lower ATPase activity than the α isoform,[46] and the isoform shift in AB is thereby expected to slow twitch kinetics despite enhanced $Ca^{2\pm}$ handling and unaltered $Ca^{2\pm}$ sensitivity. Thus, our findings indicate that the effects of passive stiffening, in combination with a myosin heavy chain shift, can outweigh the benefits of enhanced diastolic $Ca^{2\pm}$ handling.

It was beyond the scope of our study to investigate the driving mechanism for titin hypophosphorylation and collagen deposition. However, previous studies have indicated that the TGFβ[47] and the calcineurin/NFAT- signalling[48] pathways induce fibrosis following pressure-overload. Titin stiffening on the other hand appears to be additionally driven by metabolic risk factors, inflammation and oxidative stress.[5,39] As HFpEF is a multifactorial condition involving both pressure-overload and metabolic derangements, it is not surprising that the first paper to investigate mechanisms of myocardial stiffening in human HFpEF reported both higher titin and collagen-mediated stiffness.[49]

In conclusion, we have presently shown in a rat model that diastolic dysfunction associated with concentric hypertrophy following elevated afterload does not result from active myocardial stiffness. Rather, diastolic Ca^{2+} homeostasis is compensated in cardiomyocytes, which is expected to counteract restriction of ventricular filling due to collagen deposition and titin stiffening. These data are expected to be transferable to comparable conditions of diastolic dysfunction without comorbidities, and contrast to the previously observed active stiffening in hypertrophy and HFpEF of other aetiologies. Our results therefore indicate that the mechanisms for diastolic dysfunction in ventricular hypertrophy may be aetiology-dependent.

Supplementary material

Supplementary material is available at *Cardiovascular Research* online.

Acknowledgements

The authors thank the Section of Comparative Medicine, Oslo University Hospital Ullevål (Oslo, Norway), for animal care. Jon Riise and Per Andreas Norseng have been of invaluable help with the muscle strip experiments, and we thank Marte Avranden Kjær, Marna Lill Kjæreng and Wanja Kildal at Radiumhospitalet for technical support with the collagen histology.

Conflict of interest: none declared.

Funding

This project has received funding from the European Union's Horizon 2020 research and innovation programme (Consolidator grant, WEL) under grant agreement No 647714. Additional support was provided by European Union Project No. FP7-HEALTH-2010.2.4.2-4 ("MEDIA-Metabolic Road to Diastolic Heart Failure"), Deutsche Forschungsgemeinschaft (Reference nr: HA 7512/2-1), The South-Eastern Norway Regional Health Authority, Anders Jahre's Fund for the Promotion of Science, The Norwegian Institute of Public Health, Oslo University Hospital Ullevål, and the University of Oslo.

References

1. Borlaug BA. The pathophysiology of heart failure with preserved ejection fraction. *Nat Rev Cardiol* 2014;**11**:507–515.
2. Heinzel FR, Hohendanner F, Jin G, Sedej S, Edelmann F. Myocardial hypertrophy and its role in heart failure with preserved ejection fraction. *J Appl Physiol Physiol* 2015;**119**:1233–1242.
3. Gaasch WH, Zile MR. Left ventricular structural remodeling in health and disease: with special emphasis on volume, mass, and geometry. *J Am Coll Cardiol* 2011; **58**:1733–1740.
4. Burlew BS, Weber KT. Cardiac fibrosis as a cause of diastolic dysfunction. *Herz* 2002;**27**:92–98.
5. Linke WA, Hamdani N. Gigantic business: titin properties and function through thick and thin. *Circ Res* 2014;**114**:1052–1068.
6. Falcao-Pires I, Hamdani N, Borbely A, Gavina C, Schalkwijk CG, van der Velden J, van Heerebeek L, Stienen GJ, Niessen HW, Leite-Moreira AF, Paulus WJ. Diabetes mellitus worsens diastolic left ventricular dysfunction in aortic stenosis through altered myocardial structure and cardiomyocyte stiffness. *Circulation* 2011;**124**:1151–1159.
7. Louch WE, Stokke MK, Sjaastad I, Christensen G, Sejersted OM. No rest for the weary: diastolic calcium homeostasis in the normal and failing myocardium. *Physiology (Bethesda)* 2012;**27**:308–323.
8. Roe AT, Frisk M, Louch WE. Targeting cardiomyocyte Ca^{2+} homeostasis in heart failure. *Curr Pharm Des* 2015;**21**:431–448.
9. Selby DE, Palmer BM, LeWinter MM, Meyer M. Tachycardia-induced diastolic dysfunction and resting tone in myocardium from patients with a normal ejection fraction. *J Am Coll Cardiol* 2011;**58**:147–154.
10. Primessnig U, Schonleitner P, Holl A, Pfeiffer S, Bracic T, Rau T, Kapl M, Stojakovic T, Glasnov T, Leineweber K, Wakula P, Antoons G, Pieske B, Heinzel FR. Novel pathomechanisms of cardiomyocyte dysfunction in a model of heart failure with preserved ejection fraction. *Eur J Heart Fail* 2016;**18**:987–997.
11. Skardal K, Espe EK, Zhang L, Aronsen JM, Sjaastad I. Three-Directional Evaluation of Mitral Flow in the Rat Heart by Phase-Contrast Cardiovascular Magnetic Resonance. *PLoS One* 2016;**11**:e0150536.
12. Espe EK, Aronsen JM, Skardal K, Schneider JE, Zhang L, Sjaastad I. Novel insight into the detailed myocardial motion and deformation of the rodent heart using high-resolution phase contrast cardiovascular magnetic resonance. *J Cardiovasc Magn Reson* 2013;**15**:82.
13. Herum KM, Lunde IG, Skrbic B, Louch WE, Hasic A, Boye S, Unger A, Brorson SH, Sjaastad I, Tonnessen T, Linke WA, Gomez MF, Christensen G. Syndecan-4 is a key determinant of collagen cross-linking and passive myocardial stiffness in the pressure-overloaded heart. *Cardiovasc Res* 2015;**106**:217–226.
14. Andersson KB, Birkeland JA, Finsen AV, Louch WE, Sjaastad I, Wang Y, Chen J, Molkentin JD, Chien KR, Sejersted OM, Christensen G. Moderate heart dysfunction in mice with inducible cardiomyocyte-specific excision of the Serca2 gene. *J Mol Cell Cardiol* 2009;**47**:180–187.
15. Mork HK, Sjaastad I, Sejersted OM, Louch WE. Slowing of cardiomyocyte Ca^{2+} release and contraction during heart failure progression in postinfarction mice. *Am J Physiol Heart Circ Physiol* 2009;**296**:H1069–H1079.
16. Louch WE, Hougen K, Mork HK, Swift F, Aronsen JM, Sjaastad I, Reims HM, Roald B, Andersson KB, Christensen G, Sejersted OM. Sodium accumulation promotes diastolic dysfunction in end-stage heart failure following Serca2 knockout. *J Physiol (Lond)* 2010;**588**:465–478.
17. Thomas MJ, Sjaastad I, Andersen K, Helm PJ, Wasserstrom JA, Sejersted OM, Ottersen OP. Localization and function of the Na+/Ca2+-exchanger in normal and detubulated rat cardiomyocytes. *J Mol Cell Cardiol* 2003;**35**:1325–1337.
18. Hamdani N, Krysiak J, Kreusser MM, Neef S, Dos Remedios CG, Maier LS, Kruger M, Backs J, Linke WA. Crucial role for Ca^{2+}/calmodulin-dependent protein kinase-II in regulating diastolic stress of normal and failing hearts via titin phosphorylation. *Circ Res* 2013;**112**:664–674.
19. Kotter S, Gout L, Von Frieling-Salewsky M, Muller AE, Helling S, Marcus K, Dos Remedios C, Linke WA, Kruger M. Differential changes in titin domain phosphorylation increase myofilament stiffness in failing human hearts. *Cardiovasc Res* 2013;**99**:648–656.
20. Blaker YN, Brodtkorb M, Maddison J, Hveem TS, Nesheim JA, Mohn HM, Kolstad A, Geisler CH, Liestol K, Smeland EB, Holte H, Delabie J, Danielsen H. Computerized image analysis of the Ki-67 proliferation index in mantle cell lymphoma. *Histopathology* 2015;**67**:62–69.

21. Gattoni S, Roe AT, Frisk M, Louch WE, Niederer SA, Smith NP. The calcium-frequency response in the rat ventricular myocyte: an experimental and modelling study. *J Physiol (Lond)* 2016;**594**:4193–4224.
22. Helmes M, Trombitas K, Granzier H. Titin develops restoring force in rat cardiac myocytes. *Circ Res* 1996;**79**:619–626.
23. Zile MR, Gottdiener JS, Hetzel SJ, McMurray JJ, Komajda M, McKelvie R, Baicu CF, Massie BM, Carson PE, Investigators IP. Prevalence and significance of alterations in cardiac structure and function in patients with heart failure and a preserved ejection fraction. *Circulation* 2011;**124**:2491–2501.
24. King NM, Methawasin M, Nedrud J, Harrell N, Chung CS, Helmes M, Granzier H. Mouse intact cardiac myocyte mechanics: cross-bridge and titin-based stress in unactivated cells. *J Gen Physiol* 2011;**137**:81–91.
25. Hasenfuss G, Schillinger W, Lehnart SE, Preuss M, Pieske B, Maier LS, Prestle J, Minami K, Just H. Relationship between Na^{+}-Ca^{2+}-exchanger protein levels and diastolic function of failing human myocardium. *Circulation* 1999;**99**:641–648.
26. Paulus WJ, Tschope C. A novel paradigm for heart failure with preserved ejection fraction: comorbidities drive myocardial dysfunction and remodeling through coronary microvascular endothelial inflammation. *J Am Coll Cardiol* 2013;**62**:263–271.
27. Bers DM, Despa S, Bossuyt J. Regulation of Ca2+ and Na+ in normal and failing cardiac myocytes. *Ann N Y Acad Sci* 2006;**1080**:165–177.
28. Wanichawan P, Hafver TL, Hodne K, Aronsen JM, Lunde IG, Dalhus B, Lunde M, Kvaloy H, Louch WE, Tonnessen T, Sjaastad I, Sejersted OM, Carlson CR. Molecular basis of calpain cleavage and inactivation of the sodium-calcium exchanger 1 in heart failure. *J Biol Chem* 2014;**289**:33984–33998.
29. Zhang XQ, Qureshi A, Song J, Carl LL, Tian Q, Stahl RC, Carey DJ, Rothblum LI, Cheung JY. Phospholemman modulates Na+/Ca2+ exchange in adult rat cardiac myocytes. *Am J Physiol Heart Circ Physiol* 2003;**284**:H225–H233.
30. Beca S, Ahmad F, Shen W, Liu J, Makary S, Polidovitch N, Sun J, Hockman S, Chung YW, Movsesian M, Murphy E, Manganiello V, Backx PH. Phosphodiesterase type 3A regulates basal myocardial contractility through interacting with sarcoplasmic reticulum calcium ATPase type 2a signaling complexes in mouse heart. *Circ Res* 2013;**112**:289–297.
31. Nelson BR, Makarewich CA, Anderson DM, Winders BR, Troupes CD, Wu F, Reese AL, McAnally JR, Chen X, Kavalali ET, Cannon SC, Houser SR, Bassel-Duby R, Olson EN. A peptide encoded by a transcript annotated as long noncoding RNA enhances SERCA activity in muscle. *Science* 2016;**351**:271–275.
32. Sah R, Ramirez RJ, Kaprielian R, Backx PH. Alterations in action potential profile enhance excitation-contraction coupling in rat cardiac myocytes. *J Physiol (Lond)* 2001;**533**:201–214.
33. Louch WE, Hake J, Jolle GF, Mork HK, Sjaastad I, Lines GT, Sejersted OM. Control of Ca^{2+} release by action potential configuration in normal and failing murine cardiomyocytes. *Biophys J* 2010;**99**:1377–1386.
34. Marionneau C, Brunet S, Flagg TP, Pilgram TK, Demolombe S, Nerbonne JM. Distinct cellular and molecular mechanisms underlie functional remodeling of repolarizing K+ currents with left ventricular hypertrophy. *Circ Res* 2008;**102**:1406–1415.
35. Cazorla O, Lucas A, Poirier F, Lacampagne A, Lezoualc'h F. The cAMP binding protein Epac regulates cardiac myofilament function. *Proc Natl Acad Sci U S A* 2009;**106**:14144–14149.
36. Frisk M, Ruud M, Espe EK, Aronsen JM, Roe AT, Zhang L, Norseng PA, Sejersted OM, Christensen GA, Sjaastad I, Louch WE. Elevated ventricular wall stress disrupts cardiomyocyte t-tubule structure and calcium homeostasis. *Cardiovasc Res* 2016;**112**:443–451.
37. Cazorla O, Freiburg A, Helmes M, Centner T, McNabb M, Wu Y, Trombitas K, Labeit S, Granzier H. Differential expression of cardiac titin isoforms and modulation of cellular stiffness. *Circ Res* 2000;**86**:59–67.
38. Hamdani N, Paulus WJ. Myocardial titin and collagen in cardiac diastolic dysfunction: partners in crime. *Circulation* 2013;**128**:5–8.
39. Hamdani N, Franssen C, Lourenco A, Falcao-Pires I, Fontoura D, Leite S, Plettig L, Lopez B, Ottenheijm CA, Becher PM, Gonzalez A, Tschope C, Diez J, Linke WA, Leite-Moreira AF, Paulus WJ. Myocardial titin hypophosphorylation importantly contributes to heart failure with preserved ejection fraction in a rat metabolic risk model. *Circ Heart Fail* 2013;**6**:1239–1249.
40. van Heerebeek L, Hamdani N, Falcao-Pires I, Leite-Moreira AF, Begieneman MP, Bronzwaer JG, van der Velden J, Stienen GJ, Laarman GJ, Somsen A, Verheugt FW, Niessen HW, Paulus WJ. Low myocardial protein kinase G activity in heart failure with preserved ejection fraction. *Circulation* 2012;**126**:830–839.
41. Stroud JD, Baicu CF, Barnes MA, Spinale FG, Zile MR. Viscoelastic properties of pressure overload hypertrophied myocardium: effect of serine protease treatment. *Am J Physiol Heart Circ Physiol* 2002;**282**:H2324–H2335.
42. Wu Y, Cazorla O, Labeit D, Labeit S, Granzier H. Changes in titin and collagen underlie diastolic stiffness diversity of cardiac muscle. *J Mol Cell Cardiol* 2000;**32**:2151–2162.
43. Granzier HL, Irving TC. Passive tension in cardiac muscle: contribution of collagen, titin, microtubules, and intermediate filaments. *Biophys J* 1995;**68**:1027–1044.
44. Opdahl A, Remme EW, Helle-Valle T, Lyseggen E, Vartdal T, Pettersen E, Edvardsen T, Smiseth OA. Determinants of left ventricular early-diastolic lengthening velocity: independent contributions from left ventricular relaxation, restoring forces, and lengthening load. *Circulation* 2009;**119**:2578–2586.
45. Remme EW, Opdahl A, Smiseth OA. Mechanics of left ventricular relaxation, early diastolic lengthening, and suction investigated in a mathematical model. *Am J Physiol-Heart Circ Physiol* 2011;**300**:H1678–H1687.
46. Gupta MP. Factors controlling cardiac myosin-isoform shift during hypertrophy and heart failure. *J Mol Cell Cardiol* 2007;**43**:388–403.
47. Kuwahara F, Kai H, Tokuda K, Kai M, Takeshita A, Egashira K, Imaizumi T. Transforming growth factor-beta function blocking prevents myocardial fibrosis and diastolic dysfunction in pressure-overloaded rats. *Circulation* 2002;**106**:130–135.
48. Herum KM, Lunde IG, Skrbic B, Florholmen G, Behmen D, Sjaastad I, Carlson CR, Gomez MF, Christensen G. Syndecan-4 signaling via NFAT regulates extracellular matrix production and cardiac myofibroblast differentiation in response to mechanical stress. *J Mol Cell Cardiol* 2013;**54**:73–81.
49. Zile MR, Baicu CF, Ikonomidis JS, Stroud RE, Nietert PJ, Bradshaw AD, Slater R, Palmer BM, Van Buren P, Meyer M, Redfield MM, Bull DA, Granzier HL, LeWinter MM. Myocardial stiffness in patients with heart failure and a preserved ejection fraction: contributions of collagen and titin. *Circulation* 2015;**131**:1247–1259.